

Anchor deformations drive limit cycle oscillations in interferometrically transduced MEMS beams

David Blocher^{a,*}, Alan T. Zehnder^a, Richard H. Rand^a, Shreyasi Mukerji^b

^a Theoretical and Applied Mechanics, Cornell University, Ithaca, NY 14853, USA

^b Mechanical and Aerospace Engineering, Cornell University, Ithaca, NY 14853, USA

ARTICLE INFO

Article history:

Received 13 December 2010

Received in revised form

25 April 2011

Accepted 12 June 2011

Available online 4 October 2011

Keywords:

MEMS

Finite element method

Resonator

Dynamical systems

Limit cycle

Hopf

ABSTRACT

A micro-scale resonator suspended over a substrate and illuminated with a continuous wave (CW) laser forms an interferometer which couples deflection of the resonator to light absorption. In turn, absorption creates temperature and thermal stress fields which feedback into the motion. Experiments have shown that this coupling can lead to limit cycle oscillations in which the resonator vibrates in the absence of external forcing. However, the mechanism by which the thermal stresses drive limit cycle oscillations of initially flat beams was unknown. In this paper, we present a thermo-mechanical finite element method (FEM) analysis of doubly clamped beams which shows that the combination of anchor point thermal gradients and deflection due to compression couples out-of-plane motion of the beam to the thermal field. It is this coupling that makes limit cycle oscillations of the beam resonators possible. Results of the FEM analysis are used to compute the threshold laser power needed for limit cycle oscillations.

© 2011 Elsevier B.V. All rights reserved.

1. Introduction

Resonant microelectromechanical systems (MEMS) have been proposed and demonstrated for a number of different sensing [1], and signal processing [2,3] applications in the past decade. Such devices are typically lithographically defined out of thin films of silicon and silicon compounds, materials which have low mechanical losses. As a result of their small size and low inherent damping, these micro-scale beams, disks, and domes may exhibit extremely high resonant frequencies ($\omega_r \geq 1\text{GHz}$) and high quality factors ($Q \geq 100,000$). Applications such as mass sensing and signal processing depend on MEMS resonators' high-Q, high frequency oscillation and their ease of integration with traditional electronics.

In order to induce vibrations, devices are often excited electrostatically, piezoelectrically, magnetically or optically with an externally modulated input signal. However, such methods require an independent, highly stable periodic drive signal and may require additional conductive layers on the resonator surface which reduce the quality factor. Interferometric transduction can drive self-oscillation without needing an independent periodic drive signal nor additional device layers, making it a promising technique for enabling sensing and signal processing applications.

Langdon and Dowe [4] first demonstrated interferometrically transduced self-oscillation in a MEMS device. They showed that an optically thin aluminized polyester beam suspended over a reflective substrate sets up a Fabry-Pérot interferometer which couples absorption in the beam to deflection of it. If illuminated with a CW unmodulated laser, the beam bends statically for low laser power, but for high enough power ($P > P_H$) the beam begins to self-oscillate at finite amplitude.

Oscillation of the device through the interference field also modulates the intensity of reflected light which may be measured and analyzed to determine the motion [5]. In laboratory experiments, samples are mounted in a vacuum chamber evacuated to $< 10^{-6}$ mbar to reduce viscous damping, a CW laser is focused on the center of the beam and the reflected signal measured with a high speed photodiode and analyzed on a spectrum analyzer (see Fig. 1). Such experiments [6] can show the existence of hysteresis, i.e. once oscillating, the device will continue to oscillate even as the laser power is reduced until a lower power $P_L < P_H$ at which point the vibration ceases.

For interferometric transduction to be a viable means of driving MEMS resonators, the mechanisms and conditions for self-oscillation must be understood. Early work focused on beams with thin metal coatings on their top surface and suggested two possible mechanisms for self-excitation. Churenkov [7] assumed that bending moments in the beam were due to the differing thermal expansion coefficients of the beam material and surface coating. Langdon and Dowe [4] assume that the laser power is absorbed near

* Corresponding author. Tel.: +1 607 255 0824; fax: +1 607 255 2011.
E-mail address: dbb74@cornell.edu (D. Blocher).

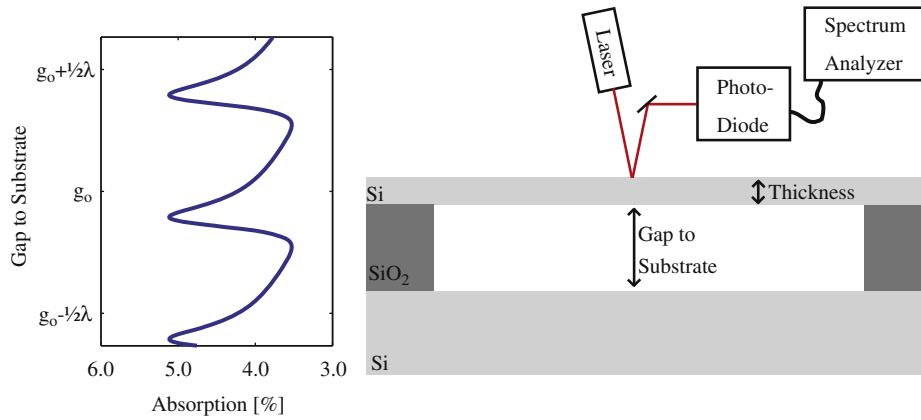


Fig. 1. Absorption in a Fabry–Pérot interferometer. Undelected beams are a distance g_0 away from the substrate at their center. Deflection of the beam changes the gap to substrate, altering the absorption in the interferometer, thus coupling absorption to deflection.

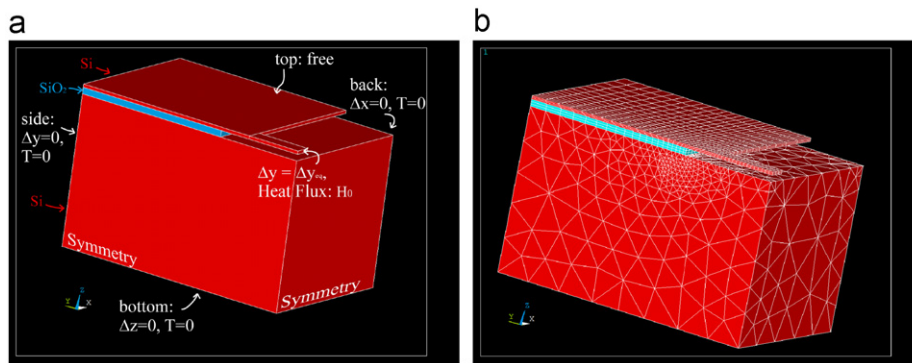


Fig. 2. Structural and thermal (a) boundary conditions as well as (b) mesh for a FEM model of a $7\ \mu\text{m}$ beam. For each model, the precise temperature field and displacement due to steady state heating was calculated using a very fine mesh. Then the mesh coarsened such that maximum temperature and vertical component of the midline displacement were accurate to within 2%. This mesh convergence study indicated the need for a high density of elements at the support.

the top surface of the beam causing vertical thermal gradients throughout the beam and deflection due to resultant bending moments. Both use energy methods to derive formulae for the minimum power needed for self-oscillation. However neither mechanism is applicable here. For uncoated beams there is no bi-metallic effect. For optically thin beams, absorption occurs throughout the beam thickness and the combination of high aspect ratios and high thermal conductivity ensures negligible vertical thermal gradients in the beam. In addition, such methods cannot capture hysteresis loops which are experimentally observed.

Others have assumed periodic surface heating [8–10] and analyzed deflection due to thermal stress waves to give an amplitude of driven oscillation which is directly proportional to the amplitude of the modulated laser power. However, such methods are not appropriate for interferometrically transduced oscillations where input power is not modulated externally, but rather by motion of the device. These self-oscillations begin at finite amplitude only after the threshold laser power is reached. Models [6,11] which display hysteresis have been used to accurately predict threshold powers for self-oscillation in specific devices. However, model parameters have not been systematically studied, nor tied to the physical mechanisms underlying deformation. Such analysis would support design questions such as—*How does one construct a MEMS resonator to have a low threshold power for self-oscillation?*

These models show that the threshold power for self-oscillation in MEMS devices depends on the direct feedback between static heating and displacement, yet it is unclear what mechanism causes the displacement. In this paper, a (FEM) model of a doubly

supported beam subject to steady state heating is analyzed using the commercially available software package, ANSYS. Results show that deflection due to heating comes from a combination of thermal gradients and compressive stresses at the beam's support. We then illustrate the importance of this direct thermal–mechanical coupling mechanism in driving interferometrically transduced self-oscillation.

2. Materials and methods

The analysis will model doubly clamped beams fabricated out of silicon–silicon dioxide–silicon (SOI) wafers. The beams are $7, 10, 15$ or $20\ \mu\text{m}$ long, $201\ \text{nm}$ thick, and $2\ \mu\text{m}$ wide with $2\ \mu\text{m}$ of undercutting and a $400\ \text{nm}$ gap to substrate. Resonant frequencies are measured to be $17.2, 10, 5.0$ and $3.6\ \text{MHz}$, respectively. SEM images show that the $20\ \mu\text{m}$ beams are post-buckled, indicating a residual compressive pre-stress σ_{res} in the device layer that is greater than the buckling load (σ_b) of the $20\ \mu\text{m}$ beam and less than that of the $15\ \mu\text{m}$ beams. Thermal–mechanical coupling is found to be highly dependent on the pre-stress, so a careful analysis of the buckling loads is done to bracket the pre-stress in the devices. To estimate the buckling loads and study the thermal–mechanical coupling, FEM models of each beam were built incorporating the beam and a large portion of the surrounding substrate. Quarter symmetry was used to reduce the problem size.

Thermal and mechanical boundary conditions for the model are shown in Fig. 2(a). In order to account for the estimate pre-stress, the corresponding strain was calculated and equivalent

step displacement Δy_{eq} applied to the midline cross section. Symmetry, clamped or free boundary conditions were applied to the remaining surfaces of the model. We assume that the laser is focused on the center of the beam. Given that the devices are optically thin, absorption is not confined to the top surface. Thus we consider the power to be evenly absorbed throughout the thickness of the beam, and apply a heat flux H_0 equivalent to 1 mW of incident laser power (4.4% absorbed) to the midline cross section. The substrate outside the model is assumed to be an infinite heat sink, and since devices operate in vacuum, with small temperatures above ambient, convective and radiative heat loss are negligible. A representative mesh is depicted in Fig. 2(b), and the material properties used are listed in Table 1.

Recall that pre-stress in our devices is bracketed by the buckling loads (σ_b) of the 15 μm and 20 μm beams. In order to calculate σ_b for each beam, the temperature is fixed at zero and the midline displacement is varied in a large deflection static analysis (NLGEOM ON, PSTRES ON) to produce a load curve. Note that the top of the device layer is surrounded by vacuum, while the bottom of the device layer is bonded to the underlying oxide layer. This geometric asymmetry of the anchor support is captured in the boundary conditions imposed in the model and causes imperfection buckling. Since the top surface of the device layer is free, shear stresses develop along the bottom of the device layer in the region of the support to counteract axial compressive stresses due to pre-stress. These shear stresses act below the beam centerline and tend to arch the beam up away from the substrate. Once the compressive stress reaches a critical load (σ_b), the growth becomes dramatic (see Fig. 3). This load is slightly less than the buckling load predicted by a Euler–Bernoulli beam theory model of an initially straight clamped–clamped beam. Analysis of the 15 μm and 20 μm beams indicates the presence of 55 ± 10 MPa of compressive pre-stress.

Having estimated the pre-stress, we apply equivalent step displacements Δy_{eq} to each beam, and calculate the midline displacement due to pre-stress alone using a large-deflection static analysis (NLGEOM, ON) which accounts for geometric non-linearities. In addition, we select (PSTRESS, ON) so that the stiffness matrix

Table 1

Material properties used in analyses. Listed from left to right are the density (ρ), Poisson ratio (ν), Young's modulus (E), coefficient of thermal expansion (α_T), thermal conductivity (k) and specific heat capacity (c). Note the two order of magnitude difference between the thermal conductivity of Si and SiO₂.

Material	ρ (kg/m ³)	ν	E (GPa)	α_T (K ⁻¹)	k (W/m K)	c (J/kg K)
Si	2420	0.279	130	2.5×10^{-6}	170	712
SiO ₂	2200	0.17	70	0.5×10^{-6}	1.38	1120

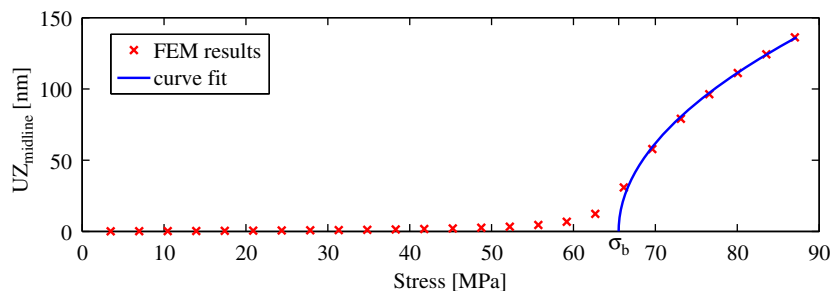


Fig. 3. Load curve for the 15 μm beam. Note that undercutting artificially softens the beam support reducing the buckling load and resonant frequency, thus making the beam “effectively” longer. For shorter, stiffer beams (7 μm) where undercutting of the length, this effect is pronounced. By comparing the FEM calculated first mode frequency of each beam with the clamped–clamped theoretical frequency [12] we calculate effective lengths of 9.44, 11.83, 16.43, and 20.9 μm . The equivalent length is used to relate stress to displacement from $\Delta y = \sigma L/2E$ and to approximate the buckling stress for the 7, 10 μm beams where a full non-linear FEM buckling analysis was not done. Thermal–mechanical coupling is found to depend critically on residual pre-stress, particularly in the neighborhood of σ_b (see Section 5). Thus careful analysis of σ_{res} is required. To find the buckling load (σ_b), we curve fit the post-buckled load curve to a square root.

is recalculated in the deformed configuration. Next we turn our attention to the thermal model. A steady state thermal analysis is performed to calculate the temperature distribution in the beam. Equivalent structural loads are applied by switching the element type from thermal to structural and the large deformation static problem including pre-stress effects is solved to find the vertical component of the midline displacement due to pre-stress and heating. The difference between these displacements, ΔUZ , provides us a measure of the thermal–mechanical coupling.

3. Results

In doubly supported beams, deflection due to heating is the result of two competing effects. Heat propagates more efficiently in the device layer because the thermal conductivity of silicon is two orders of magnitude higher than that of the underlying silicon dioxide layer [9,10]. Heat from the laser, applied at the center of the beam travels along the beam and is sunk by flowing into the low conductivity oxide. This sets up a large vertical temperature gradient in the oxide near the support (Fig. 4(a)). The device layer, being hotter than the oxide layer expands more, and the mismatch in thermal expansion coefficients between the layers (see Table 1) augments this affect to create a bending moment that tends to rotate cantilevered beams down toward the substrate. However, in doubly supported beams compressive stresses across the length of the device due to pre-stress or thermal expansion have the opposite effect: a phenomenon noted in the previous section. For the beams studied, the effect of the thermal compressive force dominates the effect of the vertical thermal gradients, causing the beams to arch up away from the substrate when heated. Assuming small displacements, we define the thermo-mechanical coupling coefficient as

$$D = \frac{\Delta UZ}{T_{ave}} \quad (1)$$

where ΔUZ is the vertical component of the displacement at the center of the beam and T_{ave} is the average temperature in the beam. Note that in calculating the coupling, we include only the displacement due to heating, not the portion due to pre-stress. This coefficient is roughly equivalent to the local slope of the load–displacement curve in Fig. 3 where excess temperature is transformed to thermal stress load. Note that the analysis is inherently non-linear in σ_{res} and H_0 . See Table 2 for a list of results. The 20 μm beams being post-buckled, have the greatest thermal–mechanical coupling (highest slope), while the 15 μm beams being nearly buckled have the second greatest thermal–mechanical coupling.

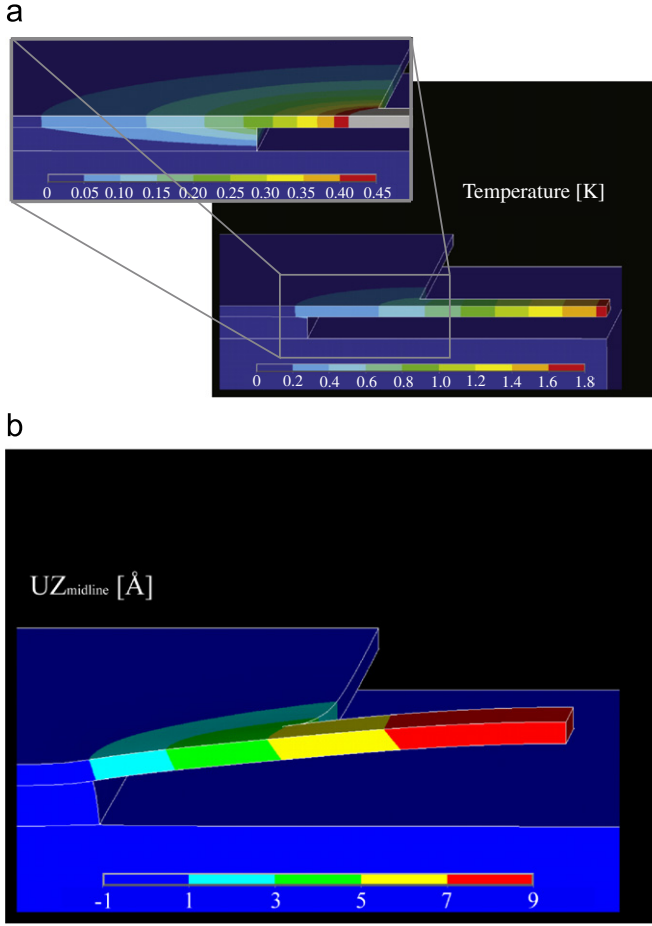


Fig. 4. (a) Temperature distribution and (b) deflection for the 7 μm beam under steady state heating—note that a portion of the displacement is due to pre-stress.

Table 2

FEM results of thermal–mechanical analysis. $\Delta UZ_{\text{midline}}$ is the vertical component of the displacement at the center of the beam due to heating with reference to the pre-stress configuration. Note that the thermal–mechanical coupling coefficient (D) increases with length.

Length (μm)	7	10	15	20
ΔUZ (\AA)	0.0364	0.0930	2.17	33.6
T_{ave} (K)	0.831	1.07	1.48	1.88
D ($\text{\AA}/\text{K}$)	0.0219	0.0434	0.734	8.96

4. Discussion

We do not sweep the laser power in the FEM model directly in order to determine the threshold power for self-oscillation because of the computational cost of solving the coupled thermal–mechanical problem. Rather, we build on past work by using our FEA results to populate parameters in a simple analytic model which has already been studied. Variations of the model have been presented in [6,13–15,11], and the interested reader should refer there for more details on its derivation. Although physical devices have spatially varying fields, first mode vibration is assumed and the midline displacement (z) is modeled as a one degree-of-freedom oscillator. The average temperature in the device (T) is modeled using a lumped thermal model. Note that heating causes compression which changes the stiffness to out of plane loads giving us a temperature dependent linear stiffness $k = k_0(1 - T/T_{\text{buckle}})$, with $T_{\text{buckle}} = (\sigma_b - \sigma_{\text{res}})/\alpha_T E$, the temperature at which a Euler–Bernoulli beam buckles due to thermal stresses. This relationship recovers exactly the frequency-compression

relationship for pre-buckled beams [12] and is approximately correct for post-buckled beams [16]. Furthermore, the slope of a load vs. displacement curve increases with displacement due to membrane stresses, giving a cubic stiffness βz^3 [17]. Including damping and the thermal–mechanical coupling term, as well as non-dimensionalizing time by the beam’s measured resonant frequency and non-dimensionalizing displacement by the laser wavelength, we get the following model of the first translational mode of vibration:

$$\ddot{z} + \frac{\dot{z}}{Q} + \left(1 - \frac{T}{T_{\text{buckle}}}\right)z + \beta z^3 = DT \quad (2)$$

The average temperature is assumed to change according to Newton’s law of cooling, giving

$$\dot{T} = -BT + HP_{\text{absorbed}}(z) \quad (3)$$

where H is the inverse of the lumped thermal mass, B is the cooling rate due to conduction, and $P_{\text{absorbed}}(z)$ is the laser energy absorbed as a function of deflection. This final term describes the Perot–Fabrey interferometer and is often modeled as

$$P_{\text{absorbed}}(z) = P(\alpha + \gamma \sin^2(2\pi(z - z_0))) \quad (4)$$

with α , γ and z_0 fitting parameters that depend on the device thickness and material properties, and P the incident CW laser power. Optical parameters (α , γ , z_0) are fit using a physics based model of reflection, transmission and absorption in thin films given in [18]. Thermal parameters (H , B) are fit using an FEM thermal model of the beam and surrounding substrate. Structural parameters (Q , T_{buckle} and β) are fit using a mixture of experimental results, analytic results, and FEM modeling. See [13] for a detailed description of the parameter estimation techniques.

Finally, we examine the nature of solutions to Eqs. (2)–(4) to identify the laser power at which self-oscillation is first seen (P_H) and at which self-oscillation ceases when reducing power (P_L). Equilibrium and periodic solutions are calculated using numerical continuation with AUTO2000 [19,20]. Numerical continuation allows us to efficiently determine whether self-oscillation is possible in the model for a given laser power. Using AUTO, we track changes in the equilibrium solution as the laser power, P , is varied, monitoring for a Hopf bifurcation. Then we restart the continuation at the Hopf bifurcation, tracking the periodic solution that emerges. As an example, parameters estimated for the 15 μm beam are listed in Table 3, and continuation results depicted in Fig. 5.

Interferometric transduction depends on the feedback between heating and displacement, yet with no direct thermal–mechanical coupling term, $D=0$, as laser power (P) increases, the displacement is zero until the beam thermally buckles at $T = T_{\text{buckle}}$. Direct thermal–mechanical coupling due to deformation of the beam supports couples heating and displacement at all temperatures making vibration possible sooner. As an example calculation, for the 15 μm beams

Table 3

Parameters for 15 μm beam. The thermal–mechanical coupling coefficient has been non-dimensionalized.

Parameter	Value
Q	10,900
H	5570 (K/W)
α	0.035
β	6.72
D	2.32×10^{-4} (1/K)
ω_r	4.975 (MHz)
B	0.112
γ	0.011
T_{buckle}	28 (K)
P	Continuation parameter

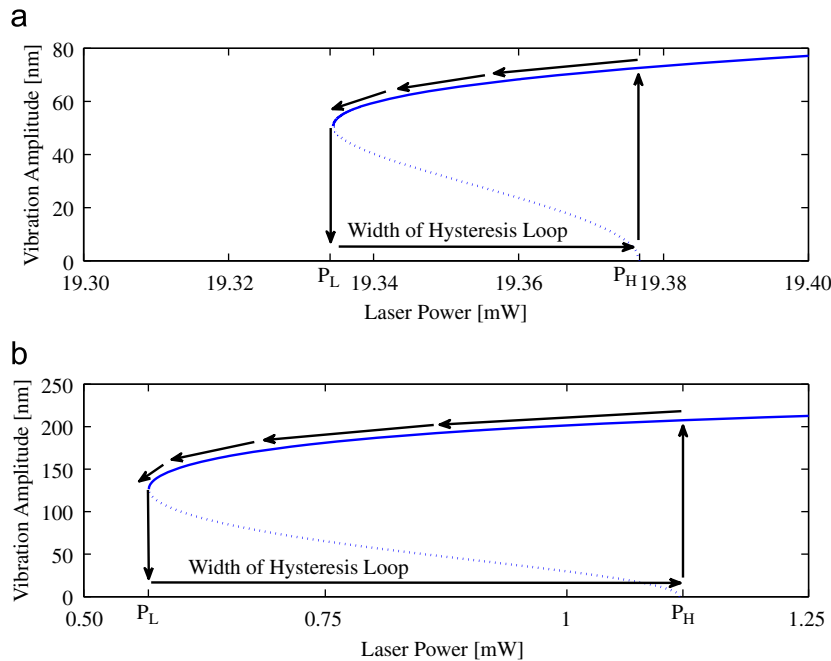


Fig. 5. Continuation of periodic solutions. Incident laser power (P) is plotted along the x -axis and the amplitude of oscillation is plotted along the y -axis. P_L is the lower threshold of self-oscillation, and P_H is the point at which the steady state solution becomes unstable giving rise to self-oscillation. Note the hysteresis loop. In addition to reducing P_H , direct thermal–mechanical coupling reduces P_L and thus increases the width of our hysteresis loop. (a) No optothermal forcing, i.e. $D=0$ in Eq. (2). (b) With optothermal forcing, i.e. $D \neq 0$ in Eq. (2).

Table 4

Model predictions of power at which self-oscillation is first seen (P_H) and lowest power for which self-oscillation is possible (P_L). For 55 MPa of pre-stress, the 20 μm beams are already buckled. For post-buckled beams, there is no self-oscillation in the model without direct thermal–mechanical coupling, and with direct thermal–mechanical forcing, the Hopf Bifurcation is supercritical and so there is no hysteresis loop. For 35 MPa pre-stress, all of the beams are pre-buckled. As a result their thermal–mechanical coupling coefficients (D) are lower and threshold power for self-oscillation (P_H) higher.

Length (μm)	No DT		With DT, $\sigma_{res} = 55$ MPa		With DT, $\sigma_{res} = 35$ MPa	
	P_H (mW)	P_L (mW)	P_H (mW)	P_L (mW)	P_H (mW)	P_L (mW)
7	482	467	64.7	19.1	76	22
10	239	233	18.2	4.46	26	5.8
15	19.4	19.3	1.12	0.568	7.0	2.0
20	N/A	N/A	0.0798	N/A	0.29	0.22

the reduction in the laser power at Hopf bifurcation (P_H) is from $P_H=19.4$ mW to $P_H=1.12$ mW.

We have used continuation to calculate P_H and P_L for the 7,10,15 and 20 μm long beams: the results are presented in Table 4. Predicted threshold powers for self-oscillation are consistent with those measured in similar sized beams [18], paddles [21], disks [15], and the predictions of Langdon and Dowe [4]. Experimental results from the actual devices modeled are forthcoming.

In order to illustrate the sensitivity of this analysis to the pre-stress values, the thermal–mechanical coupling coefficient is re-calculated, and continuation performed assuming 35 MPa of pre-stress. For this pre-stress value, all beams are pre-buckled. Note the sensitivity of (P_H) to the pre-stress value, particularly in the neighborhood of the buckling length.

5. Conclusion

When illuminated with a CW laser, MEMS resonators have been shown to go into self-oscillation for sufficiently high laser

power. Such interferometric transduction is driven by the coupling of heating to displacement and provides a means to achieve vibration in MEMS sensors without the need for externally modulated drive signals or extra fabrication steps which reduce the mechanical quality factor. We have shown that the threshold laser power needed for self-oscillation (P_H) depends intimately on the static deflection due to steady state heating, and calculated that deflection for doubly supported beams of various lengths. Unlike cantilevered beams, doubly supported beams are seen to deflect away from the substrate when heated due to compressive stress across the length of the device. We have interpreted the thermal–mechanical coupling as the slope of a imperfection buckling load curve, and shown that the power needed for self-oscillation decreases for increasing coupling. Thus, the amount of pre-stress provides a control parameter in designing low-power devices. Barely post-buckled beams should have the lowest threshold power for self-oscillation, though that power (and the operating frequency) are sensitive to changes in pre-stress near the buckling load.

Acknowledgments

This work is supported under NSF Grant #0600174 and was performed in part at the Cornell NanoScale Facility, a member of the National Nanotechnology Infrastructure Network, which is supported by the National Science Foundation (Grant ECS-0335765). This work also made use of the Cornell Center for Materials Research Facilities supported by the National Science Foundation under Award Number DMR-0520404.

References

- [1] B.R. Ilic, D.A. Czaplowski, H.G. Craighead, P. Neuzil, C. Campagnolo, C.A. Batt, Mechanical resonant immunospecific biological detector, Appl. Phys. Lett. 77 (2000) 450–452. doi:10.1063/1.127006.
- [2] A. Uranga, J. Verd, J. López, J. Teva, G. Abadal, F. Torres, J. Esteve, F. Pérez Murano, N. Barniol, Fully integrated MIXLER based VHF CMOS-MEMS

- clamped–clamped beam resonator, *Electron. Lett.* 48 (8) (2007) 452–454. doi:10.1049/el:20070580.
- [3] L. Lin, R.T. Howe, A.P. Pisano, Microelectromechanical filters for signal processing, *J. Microelectromech. Syst.* 7 (3) (1998) 286–294. doi:10.1109/84.709645.
- [4] R. Langdon, D. Dowe, Photoacoustic oscillator sensors, in: *SPIE Conference on Fiber Optic Sensors*, 1987, pp. 86–93.
- [5] D.W. Carr, L. Sekaric, H.G. Craighead, Measurement of nanomechanical resonant structures in single crystal silicon, *J. Vac. Sci. Technol. B* 16 (6) (1998) 3821–3824. doi:10.1116/1.590416.
- [6] K.L. Aubin, M.K. Zalalutdinov, T. Alan, R.B. Reichenbach, R.H. Rand, A.T. Zehnder, J.M. Parpia, H.G. Craighead, Limit cycle oscillations in CW laser-driven NEMS, *J. Microelectromech. Syst.* 13 (6) (2004) 1018–1026. doi:10.1116/1.151.6977.
- [7] A. Churenkov, Photothermal excitation and self-excitation of silicon microresonators, *Sens. Actuators A* 39 (1993) 141–148. doi:10.1016/0924-4247(93)80211-X.
- [8] R.M. Fatah, Mechanisms of optical activation of micromechanical resonators, *Sens. Actuators A* 33 (1992) 229–236.
- [9] B.R. Ilic, S. Krylov, M. Kondratovich, H.G. Craighead, Optically actuated nanoelectromechanical oscillators, *IEEE J. Sel. Top. Quantum Electron.* 13 (2) (2007) 392–399. doi:10.1109/JSTQE.2007.894190.
- [10] B.R. Ilic, S. Krylov, H.G. Craighead, Theoretical and experimental investigation of optically driven nanoelectromechanical oscillators, *J. Appl. Phys.* 107 (2010). doi:10.1063/1.3305464.
- [11] M.K. Zalalutdinov, J.M. Parpia, K.L. Aubin, H.G. Craighead, T. Alan, A.T. Zehnder, R.H. Rand, Hopf bifurcation in a disk-shaped NEMS, in: *Proceedings of the 2003 ASME Design Engineering Technical Conferences, 19th Biennial Conference on Mechanical Vibrations and Noise*, Chicago, IL, 2003, pp. 1759–1769.
- [12] S.P. Timoshenko, *Vibration Problems in Engineering*, 3rd ed., D. Van Nostrand Company, Inc., 1955.
- [13] T. Sahai, R.B. Bhiladvala, A.T. Zehnder, Thermomechanical transitions in doubly-clamped micro-oscillators, *Int. J. Non-Linear Mech.* 42 (4) (2007) 596–607. doi:10.1016/j.ijnonlinmec.2006.12.009.
- [14] M. Pandey, K.L. Aubin, M.K. Zalalutdinov, R.B. Reichenbach, A.T. Zehnder, R.H. Rand, H.G. Craighead, Analysis of frequency locking in optically driven MEMS resonators, *J. Microelectromech. Syst.* 15 (6) (2006) 1546–1554. doi:10.1109/JMEMS.2006.879693.
- [15] M.K. Zalalutdinov, A.T. Zehnder, A. Olkhovets, S.W. Turner, L. Sekaric, B.R. Ilic, D.A. Czaplewski, J.M. Parpia, H.G. Craighead, Autoparametric optical drive for micromechanical oscillators, *Appl. Phys. Lett.* 79 (5) (2001) 695–697. doi:10.1063/1.1388869.
- [16] S. Bouwstra, B. Geijselaers, On the resonance frequency of microbridges, in: *Digest of Technical Papers, Solid-State Sensors & Actuators (Transducers'91)*, 1991, pp. 538–542. doi:10.1109/SENSOR.1991.148932.
- [17] J.G. Easley, Nonlinear vibration of beams and rectangular plates, *J. Appl. Math. Phys.* 15 (1964) 167–175. doi:10.1007/BF01602658.
- [18] L. Sekaric, *Studies in NEMS: Nanoscale Dynamics, Energy Dissipation, and Structural Materials*, Ph.D. Thesis, Cornell University, 2003.
- [19] E.J. Doedel, R.C. Paffenroth, A.R. Champneys, T.F. Fairgrieve, Y.A. Kuznetsov, B.E. Oldeman, B. Sandstede, X. Wang, *AUTO 2000: Continuation and Bifurcation Software for Ordinary Differential Equations (with HomCont)*, 2002, available at <<http://indy.cs.concordia.ca/auto/>>.
- [20] E.J. Doedel, Lecture notes on numerical analysis of nonlinear equations, in: B. Krauskopf, H.M. Osinga, J. Gálan-Vioque (Eds.), *Numerical Continuation Methods for Dynamical Systems: Path Following and Boundary Value Problems*, Springer, 2007, pp. 1–49.
- [21] L. Sekaric, M.K. Zalalutdinov, S.W. Turner, A.T. Zehnder, J.M. Parpia, H.G. Craighead, Nanomechanical resonant structures as tunable passive modulators of light, *Appl. Phys. Lett.* 80 (19) (2002) 3617–3619. doi:10.1063/1.1479209.